Challenges in Automated Detection of Cervical Intraepithelial Neoplasia

Yeshwanth Srinivasan[a], Shuyu Yang[a], Brian Nutter[a], Sunanda Mitra[a], Benny Phillips[b], Rodney Long[c]

[a]Department of Electrical and Computer Engineering, Texas Tech University, Lubbock TX 79409;
[b]OB/GYN-Lubbock, School of Medicine, Lubbock, Texas 79430;
[c]National Library of Medicine, Rockville, MD 20852

ABSTRACT

Cervical Intraepithelial Neoplasia (CIN) is a precursor to invasive cervical cancer, which annually accounts for about 3700 deaths in the United States and about 274,000 worldwide. Early detection of CIN is important to reduce the fatalities due to cervical cancer. While the Pap smear is the most common screening procedure for CIN, it has been proven to have a low sensitivity, requiring multiple tests to confirm an abnormality and making its implementation impractical in resource-poor regions. Colposcopy and cervicography are two diagnostic procedures available to trained physicians for non-invasive detection of CIN. However, many regions suffer from lack of skilled personnel who can precisely diagnose the bio-markers due to CIN. Automatic detection of CIN deals with the precise, objective and non-invasive identification and isolation of these bio-markers, such as the Acetowhite (AW) region, mosaicism and punctations, due to CIN. In this paper, we study and compare three different approaches, based on Mathematical Morphology (MM), Deterministic Annealing (DA) and Gaussian Mixture Models (GMM), respectively, to segment the AW region of the cervix. The techniques are compared with respect to their complexity and execution times. The paper also presents an adaptive approach to detect and remove Specular Reflections (SR). Finally, algorithms based on MM and matched filtering are presented for the precise segmentation of mosaicism and punctations from AW regions containing the respective abnormalities.

Keywords: Computer-aided diagnosis, cervical cancer, segmentation, Gaussian Mixture Models, matched filtering

1. INTRODUCTION

Cervical cancer is the third most common form of cancer in women, affecting over 9700 women in the United States and 493,000 women worldwide every year [1, 2], resulting in over 274,000 fatalities. Cervical cancer develops slowly and has a detectable and treatable precursor condition known as dysplasia, neoplasia or CIN. CIN can be detected through screening of women at-risk and treated to prevent the development of invasive cancer [3]. The most common cervical cancer screening tool is the Papanicolaou (Pap) smear test, which has reduced cervical cancer incidence and mortality by 70% when properly implemented [4]. However, the true sensitivity of conventional Pap smear has been reported to be as low as 51% [5], requiring multiple screenings to detect CIN, making it impractical to implement in resource-poor regions.

Optical tests, such as Visual Inspection with Acetic acid (VIA), cervicography and colposcopy [6, 7] that employ visual examination of the cervix are becoming increasingly popular as diagnostic tests. In these tests, healthcare professionals study the cervix at about one minute after application of 5% acetic acid. An area of suspected tissue around the cervix opening known as the Acetowhite (AW) region and other vascular abnormalities may appear. A permanent cervicography or colposcopy record of the cervix is often made at this time, in the form of a microfilm or digital image. The severity of the abnormalities is assessed either from the direct visualization or from the recorded image. Hence, the quality of the assessment is heavily dependant on the expertise of the physician. Even in expert hands, although the sensitivity to differentiate normal and abnormal lesions has been shown to be as high as 96%, the specificity has been shown to be very low at 48% [8]. A biopsy of abnormal regions, located using one of the optical tests, is usually

performed to confirm the presence of CIN. Because the locations are currently determined manually, they are prone to significant uncertainty owing to subjective variability and, often, due to lack of skilled personnel [9, 10, 11].

As visual examination methods become more quantitative through the incorporation of digital image acquisition and analysis, it will become increasingly useful to apply medical image processing techniques to automatically and efficiently process this data in order to accurately identify and characterize the abnormal regions of the cervix. Accurate automated systems will also eliminate subjective variability, improve reliability and repeatability of diagnosis, and also help in accurate archival of diagnosis for posterity. Such a system would enhance the power of existing colposcopes and would make them immediately useful in resource-poor regions of the world, where skilled experts are scarce.

The abnormalities due to CIN that may be observed during a colposcopy may be classified into two generic groups – AW change and vascular abnormalities. AW change is the most important of all colposcopic features, because all manifestations of CIN, unless covered by keratin, will exhibit some degree of acetowhiteness [4]. Regions of high acetowhiteness correlate with regions of higher nuclear density, caused usually by CIN. Vascular abnormalities are abnormal blood vessel structures caused by CIN. Vascular abnormalities are of three types, mosaicism, punctations and vasculature, and are usually observed in the AW region. Mosaicism is an abnormal pattern of small blood vessels suggesting a confluence of chicken-wire reddish borders forming a textured mosaic pattern [6]. Punctations are fine to coarse red dots due to stippled capillaries, seen end on. Vasculature is the name given to irregular vessels forming abrupt patterns that appear as commas, corkscrews or spaghetti. The vessels in vasculature form no specific patterns, unlike mosaicism or punctations, but often indicate an abnormal lesion.

An ideal automated system should be able to segment and assess the aforementioned abnormalities due to CIN, if not provide a more complete annotation including all types of abnormalities of clinical importance, given a raw cervicographic or colposcopic image of the cervix. In practice, however, automated diagnosis is riddled with several problems. These problems include the variability in image acquisition methods, uneven shape of the cervix, lack of unique ground truth due to inter-grader variability, variations in scale, and the presence of other biological features which hinder the delineation of abnormal lesions. In the case of cervicographic images, the digital images are obtained by scanning the microfilms, which results in poor contrast and a lack of high frequency features. An automated system that works across all these problems may be very difficult to design. However, if some assumptions are made regarding the issues, and some minimal human intervention is incorporated, it is possible to design a semi-automated system for the detection, segmentation and assessment of abnormalities due to CIN.

In the past, emphasis has been placed on the segmentation of the AW region. Specifically, in [12, 13, 14] the authors use principles from [15] to detect the AW regions as an individual "blob" on the cervix images. The problem of segmenting the AW region is treated as a probability density estimation of three multi-dimensional Gaussian mixtures, where each Gaussian in the mixture corresponds to one of three regions, AW, Columnar Epithelium (CE) or Squamous Epithelium (SE). The feature vectors used are a combination of color features from the *Lab* color space and a texture feature based on the number of similarly oriented gradients in the neighborhood of each pixel at an appropriate level of scale. In [16, 17] the authors present a boundary searching snake approach that uses image gradients and region features from images formed by a multiresolution Gaussian pyramid to delineate the AW regions. Two other methods, one based on the clustering technique of DA, and the other a fast segmentation technique based on a sequence of morphological operations, have also been presented [18].

In this paper we review three of the above techniques, the MM-based segmentation approach, the DA-based approach and the GMM-based approach. We compare and contrast their advantages and shortcomings with respect to their use in automated segmentation of the AW region. We also present methods to segment mosaicism and punctations from regions containing the respective abnormalities, and discuss the way forward for building a fully automated system for the diagnosis of CIN. The rest of the paper is organized as follows. Section 2 presents the formulation of MM-based approach for segmentation of the AW region. A novel adaptive approach for the removal and interpolation of Specular Reflections (SR) is also presented in this section. In section 3, the elements of the GMM-based model are discussed. Section 4 presents the DA-based approach for AW segmentation. The three methods are compared in section 5. Mosaicism and punctation segmentation methods are presented in section 6. Section 7 presents future work and concludes the paper.

2. SEGMENTATION USING MATHEMATICAL MORPHOLOGY

This method is motivated by the manner in which trained physicians draw AW contours. The method uses the Canny edge detector with a sequence of morphological operators to obtain the contour of the AW region. The inside of the contour is the required AW mask [18]. To detect the AW contours using the method, the Specular Reflections (SR) on the image should first be removed. SR occur due to the presence of moisture on the uneven cervix surface, which function like mirrors that directly reflect the light from the illumination source. Thus uneven parts of the cervix with high moisture content, that simply reflect the light from the source, appear as bright spots heavily saturated with white light, which are referred to as SR. Apart from camouflaging the actual features, the SR also affect the subsequent segmentation routines, and hence must be removed. However, while the crux of the SR regions may be easily spotted, the contours of the SR are often ambiguous, and it is not easy to determine the boundaries of the SR regions. At the same time, it is also important to ensure that the SR removal method does not remove too much or too little of the SR. If the SR removal method removes too little, then some very bright pixels remain in the SR-removed image, skewing the subsequent AW segmentation algorithm. If the SR removal method removes too much then it is possible that some of the interesting texture due to abnormal lesions is lost.

A simple and effective two-step process is proposed here to remove SR. The method is an extension of the SR removal procedure outlined in [18]. It is based on the observation that the non-SR pixels in the image are predominantly red leading to low green and blue values in the RGB color space, while the SR pixels are heavily saturated with white light, leading to large values for all three colors in the RGB color space. In the first step, the SR pixels are identified using mathematical morphology. The process involves morphologically opening the image using a structuring element, SE, about as large as the extent of the largest SR. This has the effect of greatly smoothing the regions of the original image, I, that fit the SE, while generally smoothing the image as such. The image here is the raw colposcopic or cervicographic image. If the opened image is I_{opened}, then subtracting it from I produces an image which predominantly contains the foreground objects in I, which in this case is the SR. An adaptive threshold is found using the Otsu method [19], which selects a threshold, T, that maximizes the distance between the intraclass variance and the interclass variance. Mathematically, the sequence of operations can be written as

$$I_{opened} = I \circ SE$$
, (1)

where $\circ$ denotes the opening operation.

$$I_{FG} = I - I_{opened}$$
(2)

$$I_{SRMask}(x,y) = \begin{cases} 1, & if\ I_{FG}(x,y) > T \\ 0 & otherwise \end{cases}$$
(3)

The size of SE is chosen adaptively by increasing it from 5x5 pixels to 25x25 pixels and choosing the size at which the maximum [R, G, B] values of the residual non-SR pixels is less than [200, 200, 200]. A maximum size of 25x25 pixels was found to be sufficient to deal with the SR sizes encountered in the dataset. While the threshold fixed for the R, G and B values is a hard threshold, it was found to apply effectively to both colposcopic and cervicographic images. The adaptive selection of the SE size eliminates user intervention to manually fix the size of the largest SR observed in the image.

In the second step, the SR pixels in I are first masked out using I_{SRMask} to obtain I_{SRRem}. Then the removed pixels in I_{SRRem} are iteratively filled using non-zero pixels in and around the neighborhood of the remaining pixels. It is necessary to iterate the filling process because during the first, or even the first few, iterations, there may be SR pixels that are completely surrounded by removed SR pixels in the neighborhood used. This final interpolated image is denoted $I_{SRInterp}$. A neighborhood size of 5x5 pixels was used for sampling the non-SR pixels around the SR removed regions. Figure 1 shows an example to demonstrate the effectiveness of the proposed approach. Figure 1(a) shows and image of the cervix, I, cropped to contain only the pathologically significant regions for CIN. Figure 1(b) shows the SR-removed image, I_{SRRem}. The SR interpolated image, $I_{SRInterp}$, is shown in figure 1(c). The size of the SE was adaptively found to be 10x10 pixels for this case.

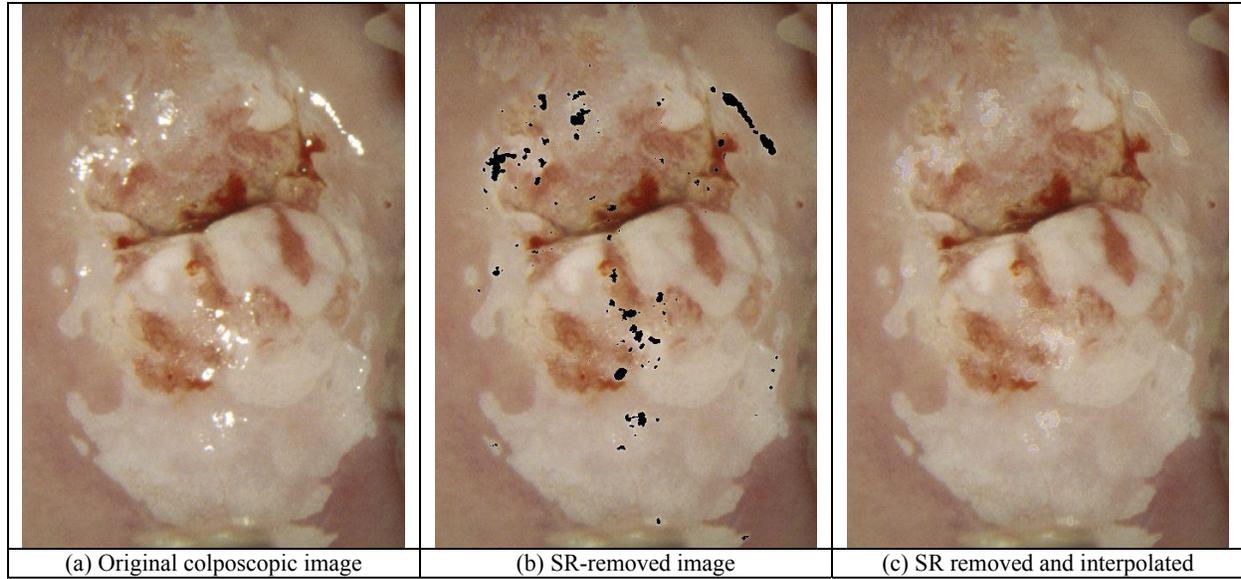| (a) Original colposcopic image | (b) SR-removed image | (c) SR removed and interpolated |

Figure 1 SR removal and interpolation

The morphological AW segmentation procedure is applied on $I_{SRInterp}$. The SR-removed image, $I_{SRInterp}$, is first converted to grayscale, I_{gray}.

$$I_{gray}(x,y) = 0.3I_{SRInterp}(x,y,1) + 0.59I_{SRInterp}(x,y,2) + 0.21I_{SRInterp}(x,y,3) \qquad (4)$$

where 1,2 and 3 represent R, G and B, respectively. A global threshold T is then computed using the Otsu method to transform the gray image I_{gray} to a binary image I_{bin}. As previously noted the Otsu method yields a threshold that maximizes the separation between inter and intra class variances and gives a general idea about the location of the AW region.

$$I_{bin}(x,y) = \begin{cases} 1 \, if \, I_{gray}(x,y) \geq T \\ 0 \, if \, I_{gray}(x,y) < T \end{cases} \qquad (5)$$

where T is the Otsu threshold. Regions disconnected from the central AW structure are removed by morphological erosion. The resulting mask is called I_{mask}.

$$I_{mask} = I_{bin} \Theta SE_E \qquad (6)$$

where Θ denotes the erosion operation and SE_E denotes a typical 3x3 structuring element consisting of ones. Other sizes may be appropriate for optimal results for specific applications.

The mask I_{mask} is superimposed over I_{gray}, to get I_{coarse}, which restricts the following operational region.

$$I_{coarse} = I_{mask} \, .* \, I_{gray} \qquad (7)$$

where '.*' indicates a pixel by pixel product. This is very useful, especially when there are potentially influential regions outside the real AW region. The image I_{edge} is then subjected to a sequence of morphological operations to obtain the AW mask. First, I_{edge} is dilated using 4 linear structuring elements oriented along 4 different angles, 0°, 45°, 90° and 135°, to get I_{dilate}.

$$I_{dilate} = \bigcup \left(I_{edge} \oplus SE_0, I_{edge} \oplus SE_{45}, I_{edge} \oplus SE_{90}, I_{edge} \oplus SE_{135} \right) \qquad (8)$$

where 'U' denotes the union operator, $\oplus$ denotes the dilation operation, and SE_0, SE_{45}, SE_{90} and SE_{135} represent linear structuring elements oriented at 0°, 45°, 90° and 135°, respectively.

The holes (black pixels) in I_{dilate} are then filled, and spurious structures along the image border are removed to get I_{filled}.

$$I_{filled} = \mathrm{Region\_fill}(I_{dilate}) \qquad (9)$$

where the 'Region_fill' function fills the black interior of a white boundary with white. Finally, a morphological closing operation is performed to get the final mask I_{AWmask},

$$I_{AWmask} = I_{filled} \bullet SE_E ,$$

(10)

where $\bullet$ denotes the morphological closing operation. The AW mask, I_{AWmask}, is applied to $I_{SRInterp}$, and the resultant image, I_{AW}, is used as the input for the next stage.

$$I_{AW} = I_{AWmask} .* I$$

(11)

For all these equations, $x \in [1, N_R]$ and $y \in [1, N_c]$, where N_R and N_C are the number of rows and columns of the image, respectively.

The results of the edge-based AW segmentation are shown in figure 2. Figure 2(a) is the SR removed and interpolated image section shown in figure 1(c), while figure 1(b) is the image with the AW contours as detected by the morphological AW segmentation approach. It can be seen that the algorithm does a fairly good job of delineating the AW regions, albeit including a significant amount of the CE region and producing some spurious AW regions in the SE region. A more detailed discussion of the approach may be found in [18].
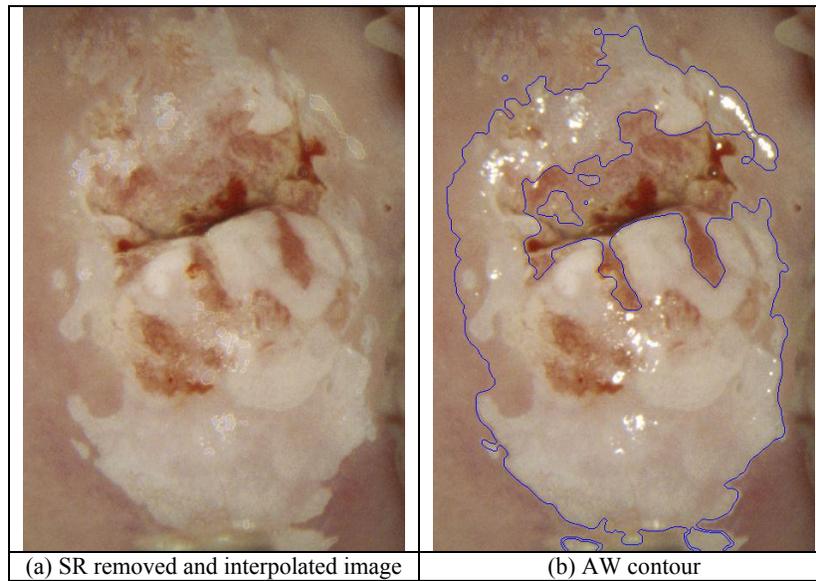
| (a) SR removed and interpolated image | (b) AW contour |

Figure 2 Segmentation using the morphological AW segmentation approach

3. SEGMENTATION USING GAUSSIAN MIXTURE MODELS

GMM are statistically mature methods of clustering. GMM work under the assumption that each d-dimensional cluster in a dataset may be modeled as a multivariate Gaussian, distribution. Hence, the complete dataset may be modeled as a mixture of these individual Gaussians. The problem of determining the clusters may then be posed as a problem of estimating the densities of the Gaussians. The basic idea with GMMs is that the probability density function of a d-dimensional random variable can be expressed as a weighted sum of K d-dimensional Gaussians. Let X = {x_1, x_2, …,x_N} be a dataset of size N, where x_i are points on a d-dimensional feature space. Then, the GMM assumption is that

$$p(x \mid \mu, \Sigma) = \sum_{j=1}^{K} \alpha_j \frac{1}{\sqrt{(2\pi)^d |\Sigma_j|}} \exp \left\{ -\frac{1}{2}(x - \mu_j)^T \Sigma_j^{-1}(x - \mu_j) \right\} ,$$

(12)

where α_j are the probabilities of occurrence of each Gaussian and μ_j and Σ_j are the mean and covariance matrix of the j-th Gaussian. For segmentation applications, since pixels in an image are allowed to belong to only one region, the maximum posteriori probability is used to assign the feature vector corresponding to each pixel to a particular cluster.

The Expectation-Maximization (EM) algorithm is a general method of finding the maximum-likelihood estimate of the parameters of an underlying distribution from a given dataset, especially when the data is incomplete or has missing

values [20, 21]. For the GMM, the EM may be used to determine α_j, μ_j and Σ_j of all the Gaussians in the mixture. The problem of segmenting the AW region in images of the cervix now becomes a problem of estimating the densities of the 3rd order GMM, where each of the three Gaussians correspond to AW, CE and SE regions. For the clusters calculated to accurately segment each desired region, the features representative of each region should be appropriately and accurately chosen. In the past, researchers have used a combination of color and texture features to model the three regions of interest [12, 13, 14]. However, the assumption that the CE region was the only textured region was found to be invalid in most cases, especially in images containing mosaicism and other vascular structures.

In this work, the choice of features was made by observing the perceptual characteristics of the cervix. Once the SR pixels are removed, the resulting image consists predominantly of three regions – CE, SE and AW. The CE region is the region immediately surrounding the os and is approximately near the center of the image. The CE region is bright red in color and is usually the darkest in the luminance plane. The AW region is the region immediately surrounding the CE region. It appears white or very pale pink depending on the intensity of acetowhiteness and is usually the brightest region in the luminance plane. The outermost region in the image is the SE region, which has a reddish hue usually between that of the CE and AW regions. Based on these observations, three features were chosen to represent the image to be segmented. To represent the difference in intensities, L from the CIE Lab color space [22] used. The difference in redness was represented by a from the Lab color space. The Euclidean distance of each point from the center of the image, d, was used to represent the difference in spatial orientation of each region. The distance feature was weighed by a factor, w, where 0<w<1, to prevent biasing the segmentation procedure from forming circular clusters. For the images used in testing, w = 0.2 was applied.

To segment the AW, CE and SE regions, the SR-removed RGB image, I_{SRRem}, is converted to Lab color space, the L and a planes smoothed to remove shot noise, and the L, a and d values are extracted from each non-SR pixel. The maximum likelihood estimate of the parameters of the 3rd order Gaussian mixture are found by applying the EM algorithm on the 3D [L, a, w*d] vectors. The EM algorithm is modified to incorporate the inter-dependence of pixels in a neighborhood. This is to imply that pixels that lie close to each other should belong to the same cluster unless they are radically different from one another in the feature space. This idea is incorporated into the EM algorithm for density estimation by smoothing the membership probabilities estimated at each E-step. Each pixel in I_{SRRem} is assigned to one of three clusters, c_k, such that c_k is the index of the Gaussian corresponding to the maximum aposteriori probability. The cluster corresponding to the Gaussian with the largest L value is always labeled as the AW region. To split between SE and CE, the distances are used. The cluster corresponding to the Gaussian with the smallest mean distance from the center is labeled as the CE region, and the remaining cluster is labeled as the SE cluster. Figure 3 shows the segmentation results for the SR-removed image shown in figure 1(b). It can be seen that the GMM-based segmentation approach provides an excellent estimate of each of the three regions.
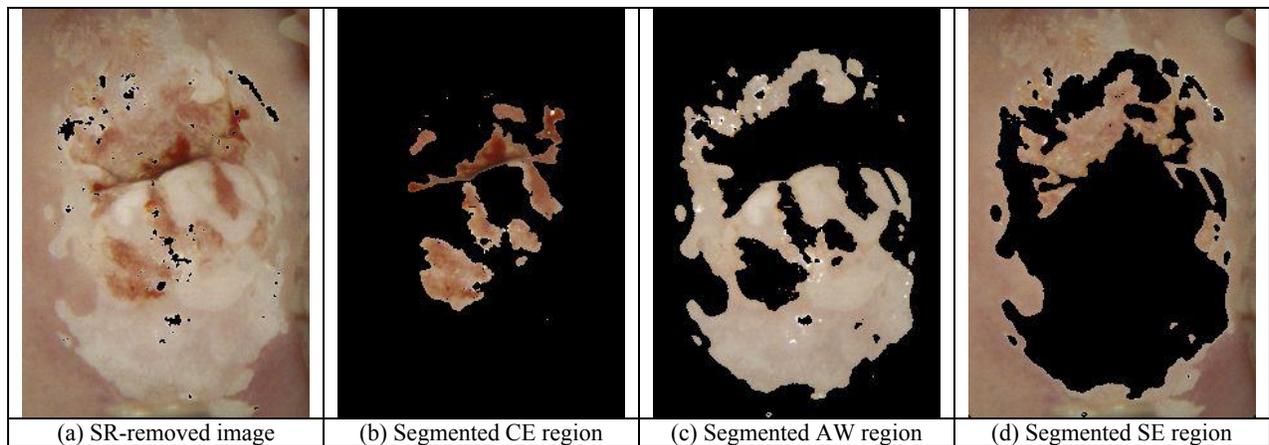

| (a) SR-removed image | (b) Segmented CE region | (c) Segmented AW region | (d) Segmented SE region |

Figure 3 Segmentation using the GMM-based approach

4. SEGMENTATION USING DETERMINISTIC ANNEALING

Deterministic annealing is an optimization algorithm based on principles of information theory and probability theory [23]. Specifically, it minimizes the expected distortion of the given system while maximizing its randomness, given by Shannon's entropy. The optimization is equivalent to minimizing the Lagrangian

$$F=D-TH, \qquad (13)$$

where T is the Lagrange multiplier, D is the distortion of the system, H is the Shannon entropy. F is minimized with respect to p(y|x), the association probability of input vector x and centroid y. The centroid values of y can be computed by an iteration that starts at large value of T, tracking the minimum while decreasing T. This statistical optimization process is analogous to the statistical mechanics annealing process when D is taken as the energy of a physical system, H its entropy and T the temperature of the system that governs the level of randomness. Minimizing the Lagrangian F is in fact tracking the minimum of the free energy while gradually lowering the temperature, which is similar to that of an annealing process. There are a couple of parameters that govern the annealing process, each exerts its influence on the outcome, particularly the temperature rate (how fast the system is cooling down).

Based on the observation that the AW region is different from other regions of the image in luminance, using DA for AW region segmentation is straight forward: The input image intensity (three color planes, i.e. red, green, and blue) is used as the only feature. Each pixel is fed into the DA clustering algorithm as a three dimensional vector. Depending on the intensity and color variation subtlety of the image, various numbers of clusters are generated with DA. The clusters fallen in the AW region is used to form the mask for segmentation. When the transition between different components is smooth, more clusters have to be generated to differentiate them. Figure 4 shows the segmented AW region of the same image (640 x 448) used in the other two methods.
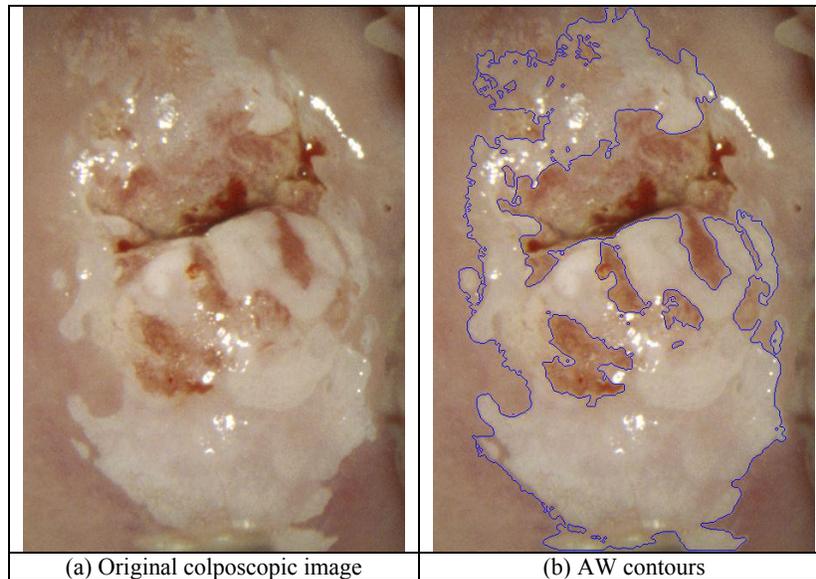

| (a) Original colposcopic image | (b) AW contours |

Figure 4 AW segmentation using DA

5. COMPARISON OF METHODS

Three different methods for segmenting the AW region were presented in the previous sections. Segmentations on four images, using the three methods are shown in figure 7. All three methods identify most of the AW regions. However, each method comes with its set of advantages and shortcomings. The MM-based approach is the fastest of the three methods, with an average operation time under 10 seconds for an image of size 640x448. However, the method sometimes tends to produce several spurious edges, evident in the first image in row 1 of figure 7. While the SE region may be estimated as the region outside the AW contour, the method does not provide an estimate of the CE regions. The GMM-based segmentation method overcomes some of these shortcomings. The GMM-based method provides estimates for the CE and SE regions in addition to estimating the AW region. The algorithm also has the ability to detect small

isolated AW regions. However, the GMM-based model restricts itself to finding regions in the image that are similar in terms of the features used, which may be inadequate if the regions are too complex to be modeled by the three simple features. The GMM-based model also operates slower than the MM-based segmentation approach, averaging about 70 seconds for a 640x448 image.

From the segmentation results it is clear that DA produces the most accurate results. However, DA may not be best suited for automated segmentation in its current form as the DA parameters have to be manually chosen based on each image. Also, DA runs very slowly; the length of time depending on the number of centroids needed to satisfactorily segment the AW region from other regions. For example, the segmentation of AW region in Figure 4 uses 8 clusters which takes 12 minutes to obtain. However, the results using DA are promising to warrant the exploration of automatically selecting the parameters for automated segmentation. Thus, of the three methods discussed, the GMM-based method offers a good compromise in terms of segmentation accuracy, model complexity and execution time. All times tests were performed on a system running AMD Athlon XP 2GHz processor with 1.5 GB RAM.

6. SEGMENTATION OF MOSAICISM AND PUNCTATIONS

Mosaicism and punctations are vascular abnormalities that are representative of a severity of CIN higher than simple AW. It is often important to segment mosaicism and punctations from sections containing the respective abnormalities to assess the inter-capillary distance, which usually increases as CIN progresses. Punctations appear as roughly circular objects with a heavy reddish hue on the RGB image or as dark objects on the corresponding grayscale image. Because the shape and size of the objects are fairly uniform and known apriori, matched filtering using a template matching the shape of the object to be detected can be used to accentuate these objects. Punctations also have a tendency to occur in groups with no clear line of demarcation between two or more punctations. Matched filtering using a Gaussian template helps to increase the degree of separation between two close punctations because the detected objects are forced to be circular. Matched filtering is implemented as a convolution given by

$$m(x,y) = G(x,y) * f(x,y),$$

(14)

where $G(x,y)$ is a separable 2-D Gaussian kernel with $\sigma = 10$, which was found to adequately describe the variations in intensity around punctations in the samples used, $f(x,y)$ is the input image, and $m(x,y)$ is the matched filtered image. Matched filtering essentially serves two purposes: it increases the contrast around individual punctations, and it smoothes uniform regions. The resulting image, $m(x,y)$, consists of dark punctations on a bright background.

The intensities of $m(x,y)$ can be modeled as a mixture of two Gaussians, one that predominantly models the variations in intensity of the punctations, and one that predominantly models the variations in intensity in the background. The maximum likelihood estimate for the parameters of the two Gaussians can be found using the EM algorithm. An important advantage of modeling $m(x,y)$ as a GMM is that it helps to make the detection algorithm independent of the image acquisition process. Because the EM algorithm is applied to each individual image, the punctations will be detected irrespective of variations in illumination and image acquisition modalities as long as the punctations appear darker than the background. Figure 5 shows an example section containing punctations and the segmented punctations. The grayscale image is pre-processed using anisotropic diffusion [24] to smooth the background while preserving the edges.

The mosaic structures can be segmented using approaches demonstrated in [25, 26]. The segmentation is based on the assumption that the mosaic structures may be modeled as a union of rotated line segments. The grayscale section containing mosaicism is enhanced by applying a morphological top-hat transform, complemented, and subject to morphological opening using a sequence of 8 rotating linear structuring elements, called ROSE for ROtating Structuring Elements. The maximum of the 8 resulting images is retained at each pixel. The resulting image is converted to a binary image using an adaptive threshold. The bright structures in the image represent the mosaic structures in the section. Figure 6 shows an example segmentation.
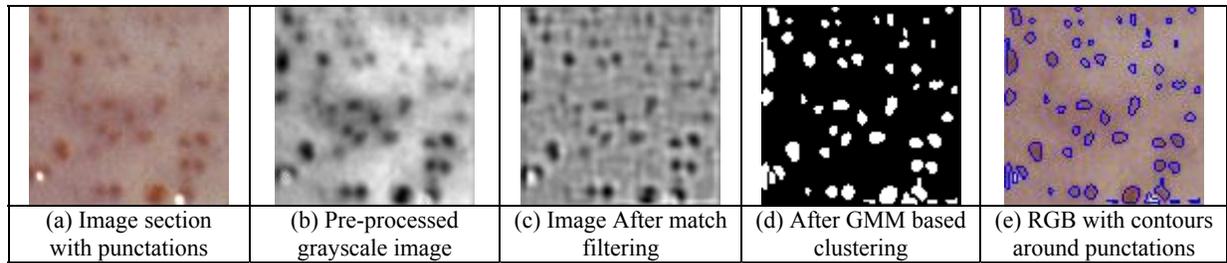
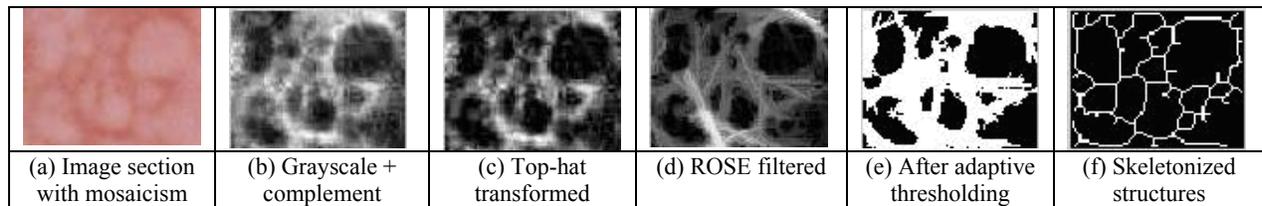| (a) Image section with punctations	(b) Pre-processed grayscale image	(c) Image After match filtering	(d) After GMM based clustering	(e) RGB with contours around punctations

Figure 5 Segmentation of punctations

(a) Image section with mosaicism	(b) Grayscale + complement	(c) Top-hat transformed	(d) ROSE filtered	(e) After adaptive thresholding	(f) Skeletonized structures

Figure 6 Segmentation of mosaicism

7. CONCLUSIONS AND FUTURE WORK

In this paper, we have compared and contrasted three methods for segmentation of the AW region from images of the cervix. The morphological AW segmentation method provides advantages in its speed, but has a tendency to produce spurious edges. The DA-based segmentation may be tuned for most accurate results, but is very slow in its operation and unsuitable for automatic segmentation in its current form. The GMM-based method provides a good compromise between the two methods with the additional advantage of also providing estimates of the CE and SE regions. A novel adaptive method for the removal of SR was also presented. The mosaic and punctation segmentation algorithms provide two additional pieces to solve the problem of complete automated diagnosis of CIN. Future research in this direction will include methods for automatically locating image sections containing vascular abnormalities, comparison of automated segmentations with ground truth segmentations marked by experts and automated disease severity assessment.

8. ACKNOWLEDGEMENTS

REFERENCES

[1] American Cancer Institute, Cancer facts and figures 2006.

[2] J. Ferlay et al., GLOBOCAN 2002: Cancer incidence, mortality and prevalence worldwide, IARC CancerBase No. 5, version 2.0 accessed online at http://www.iarc.fr/.

[3] L. G. Koss, "The papanicolaou test for cervical cancer detection. A triumph and tragedy," JAMA, Vol. 261, pp. 773-774, 1989.

[4] M. Anderson, J. Jordan, A. Morse, and F. Sharp, A text and atlas of integrated colposcopy, Chapman and Hall, First edition, 1991.

[5] D. G.Ferris, "Cervicography-An adjunct to Papanicolaou screening," Am Fam Phys., Vol. 50, pp. 363-370, 1994.

[6] E. J. Mayeaux and G. Newkirk, "Introduction to colposcopy",
http://lib-sh.lsuhsc.edu/fammed/atlases/colpoat.html, 2001.

[7] R. Sankaranarayanan and R.S. Wesley, A practical manual for visual screening for cervical neoplasia, International Agency for Research on Cancer, France, 2003.

[8] M. F. Mitchell, D. Schottenfeld, G. Tortolero-Luna, S. B. Cantor and R. Richards-Kortum, "Colposcopy for the diagnosis of squamous intraepithelial lesions: a meta-analysis," Obstetrics and Gynecology, Vol. 91, pp. 626-631, 1998

[9] L. Denny, L. Kuhn, A. Pollack, H. Wainwright, and T. C. Wright Jr., "Evaluation of alternative methods of cervical cancer screening for resource-poor settings", Cancer, Vol. 89, pp. 826-833, 2000.

[10] M. H. Schiffman, "Arguments against the routine clinical use of currently available HPV screening tests", Contemporary OB/GYN, Vol. 35, pp. 34-46, 1990.

[11] D. G. Ferris, S. Mitra, and B. Nutter, "Digitized Cervical Images: Problems, Solutions, and Potential Medical Impact," Journal of Lower Genital Tract Disease, Vol. 10, No. 1, pp. 10-15, 2006.

[12] G. Zimmerman, S. Gordon and H. Greenspan, "Content-based indexing and retrieval of uterine cervix images", Proc. of 23rd IEEE Convention of Electrical and Electronics Engineers in Israel 2004, pp. 181-185, Tel-Aviv, Israel, 2004.

[13] S. Gordon, G. Zimmerman and H. Greenspan, "Image segmentation of uterine cervix images for indexing in PACS", Proc. of the 17th IEEE Symposium on Computer-Based Medical Systems, pp. 298-303, CBMS 2004, Bethesda, MD, 2004.

[14] S. Gordon, G. Zimmerman, R. Long, S. Antani, J.Jeronimo and H. Greenspan, "Content analysis of uterine cervix images: Initial steps towards content based indexing and retrieval of cervigrams", to appear in Proc. of SPIE medical imaging, 2006.

[15] C. Carson, S. Belongie, H. Greenspan and J. Malik, "Blobworld: Image segmentation using expectation-maximization and its application to image querying", IEEE Trans. On pattern Analysis and Machine Intelligence, Vol. 24, No. 8, pp. 1026-38, Aug. 2002.

[16] V. V. Raad, "Active contour models - a multiscale implementation for anatomical feature delineation in cervical images", IEEE international Conf. on Image Proc., Vol. 1, pp. 557-560, Oct. 2004.

[17] V. V. Raad, "Active contour model based segmentation of colposcopy images from cervix uteri using Gaussian pyramids", 6th International Symposium on Digital Signal Processing for Communication Systems (DSPCS'02), pp. 133-138, Sydney, Australia, Jan. 2002.

[18] Y. Srinivasan, F. Gao, B. Tulpule, S. Yang, S. Mitra and B. Nutter, "Segmentation and classification of cervix lesions by texture and pattern analysis", Intl. Journal of Intelligent Systems Technologies and Applications, Vol. 1, Nos. 3/4, pp. 234-246, 2006.

[19] N. Otsu, "A threshold selection method from gray-level histograms," IEEE Trans. on systems, Man, and Cybernetics, SMC-8, No.1, pp. 62-66, 1979.

[20] F. Dellaert, "The expectation maximization algorithm", Georgia Institute of Technology, Technical Report Number GIT-GVU-02-20, Feb 2002.

[21] J. A. Bilmes, "A gentle tutorial to the EM algorithm and its application to parameter estimation for Gaussian mixture and hidden Markov models", International Computer Science Institute, Technical Report Number TR-97-021, Apr 1998.

[22] Hunter Labs, "CIE L*a*b* color space", Insight on Color, Vol. 8, No. 7, Jul. 1-15, 1996

[23] K. Rose, "Deterministic annealing for clustering, compression, classification, regression, and related optimization problems," Proceedings of the IEEE, Vol. 86, No. 11, Nov 1998.

[24] P. Perona, J. Malik, "Scale space and edge detection using anisotropic diffusion," IEEE Transactions on Pattern Analalysis Machine Intelligence, vol. 12, no. 7, pp. 629-639, Jul. 1990.

[25] Q. Ji, J. Engel, E. Craine, "Texture analysis for classification of cervix lesions," IEEE Transactions on Medical Imaging, Vol. 19, No. 11, 2000.

[26] B. Tupule, "Color and texture analysis of cervix lesions," Master's thesis, Texas Tech University, 2004.

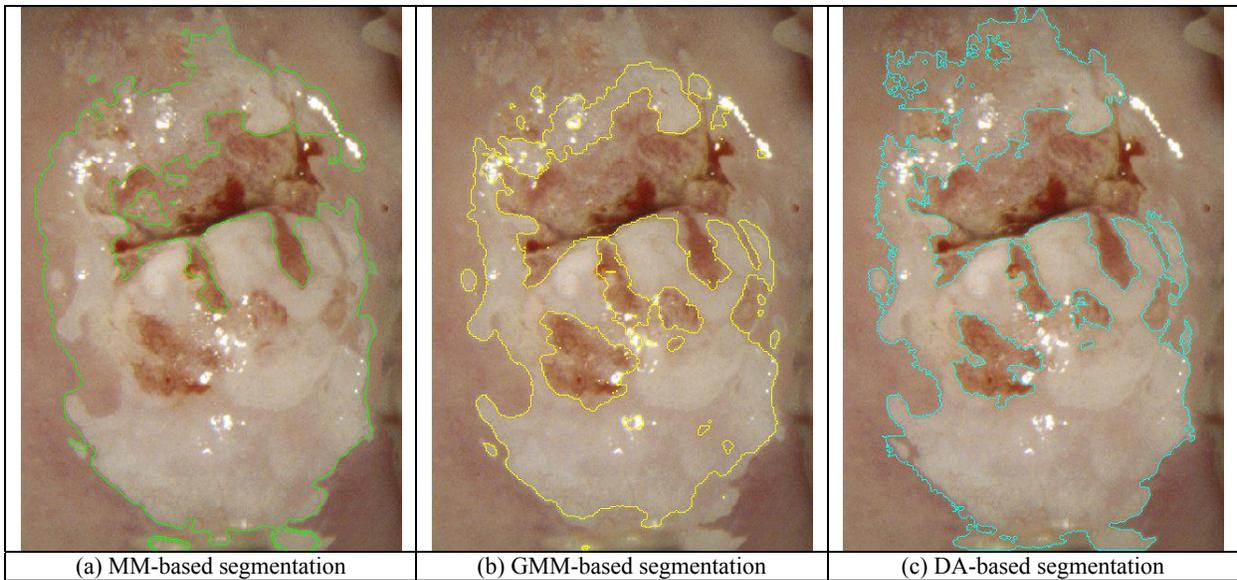| (a) MM-based segmentation | (b) GMM-based segmentation | (c) DA-based segmentation |
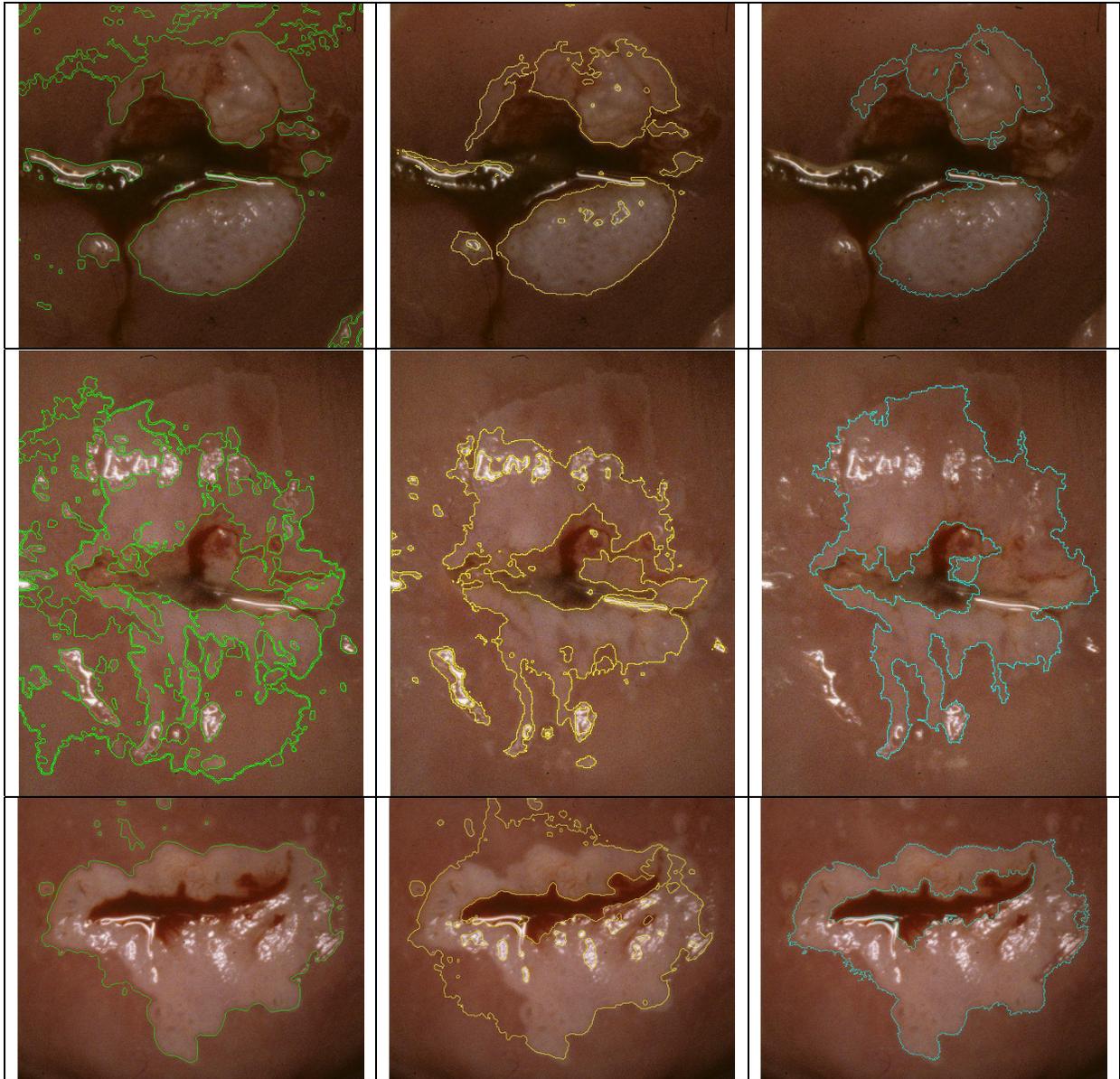
Figure 7 Comparison of AW segmentations using the three different methods